

Collective flow of light particles in Au + Au collisions at intermediate energiesYongjia Wang,^{1,2} Chenchen Guo,^{2,3} Qingfeng Li,^{2,*} Hongfei Zhang,¹ Zhuxia Li,⁴ and Wolfgang Trautmann⁵¹*School of Nuclear Science and Technology, Lanzhou University, Lanzhou 730000, P.R. China*²*School of Science, Huzhou Teachers College, Huzhou 313000, P.R. China*³*College of Nuclear Science and Technology, Beijing Normal University, Beijing 100875, P.R. China*⁴*China Institute of Atomic Energy, Beijing 102413, P.R. China*⁵*GSI Helmholtzzentrum für Schwerionenforschung GmbH, D-64291 Darmstadt, Germany*

(Received 21 May 2013; revised manuscript received 7 October 2013; published 11 March 2014)

The Skyrme potential energy density functional is introduced into the ultrarelativistic quantum molecular dynamics model and the updated version is applied to studying the directed and elliptic flows of light particles (protons, neutrons, deuterons, tritons, ^3He , and ^4He) in $^{197}\text{Au} + ^{197}\text{Au}$ collisions at beam energies 150, 250, and 400 MeV/nucleon. The results are compared with the recent FOPI experimental data. It is found that the yields and collective flows of light particles can be described quite well. The influence of the equation of state, medium-modified nucleon-nucleon elastic cross sections (NNECS) and cluster recognition criteria on the directed and elliptic flows is studied in detail. It is found that the flows of light particles are sensitive to the medium-modified NNECS, but not sensitive to the isospin dependent cluster recognition criteria. It seems difficult, however, even with the new data and calculations, to obtain a more accurate constraint on the nuclear incompressibility K_0 than the interval 200–260 MeV.

DOI: [10.1103/PhysRevC.89.034606](https://doi.org/10.1103/PhysRevC.89.034606)

PACS number(s): 25.70.-z, 24.10.-i, 25.75.Ld

I. MOTIVATION

The equation of state (EOS) of nuclear matter and the nucleon-nucleon cross sections (NNCS) in the nuclear medium have been hot topics in nuclear physics for a long time [1]. Heavy ion collisions (HICs) provide a unique opportunity to study these subjects in the laboratories around the world. It has been always difficult, however, to directly extract information on the EOS and NNCS from the measured quantities of HIC experiments because of the complexity of the collision process and the restriction of the experimental data to the asymptotic configurations recorded by the detectors. Microscopic transport theory has, therefore, been a valuable tool for simulating the dynamical process of HICs, so as to link the experimental observables to both the nuclear EOS and the in-medium NNCS [2].

The collective flow is a common phenomenon of HICs, first discovered at the LBNL Bevalac in 1984 (see Ref. [3] and references therein). The directed flow (also called in-plane or sideward flow) and the elliptic flow (also called out-of-plane flow) are two lower-order components of the flow which have been widely used for studying HICs in a large range of beam energies varying from tens of MeV up to several TeV per nucleon. Newly measured experimental data of flows were usually compared with corresponding theoretical results, calculated with the most recent updated theoretical transport models, in order to obtain further insight into the properties of the EOS and the in-medium NNCS. A large effort has been devoted to constraining the stiffness of the EOS of isospin symmetric nuclear matter, e.g., the pioneer works in Ref. [4] with sub-threshold kaon production and in Ref. [2] with collective flow observables, with the result that it is most likely soft with an incompressibility K_0 of about

230 ± 30 MeV [5]. Up to now, however, the stiffness of the EOS of isospin asymmetric nuclear matter (“ K_{asy} ”), especially at high densities, is still not well constrained, and the medium modified NNCS have not been well understood either. Thus both more precise experimental data and self-consistent theoretical models are still called for.

One of the interesting phenomena already known from early stage flow-related experiments [6–8] is the dependence of the directed and elliptic flows on the particle species. The flow effect is larger for composite particles than for protons. With the subsequent large number of experimental (see, e.g., Refs. [9–13]) and theoretical (see, e.g., Refs. [14–19]) endeavors, the presence of this effect was confirmed by observing more precisely the increase of flow with the particle mass, even though the definitions of flow and the interpretations were somewhat different in the respective studies. Recently, by using the large acceptance apparatus FOPI at the Schwerionen-Synchrotron (SIS) at GSI, a large amount of directed and elliptic flow data for light charged particles (protons, deuterons, tritons, ^3He , and ^4He) from intermediate energy HICs have been made available [20,21]. Moreover, flows are presented differentially in the FOPI data [21] in the form of both rapidity and transverse momentum distributions. Therefore, new opportunities have been opened up which will allow us to discuss the following questions:

- (i) Is it possible to reduce the uncertainty of K_0 of the EOS by comparing a large number of two-dimensional flow data with model calculations?
- (ii) Is it now possible to extract more information on the medium modifications of NNCS?
- (iii) How do different cluster recognition criteria affect the flows of light particles? This last question arises because the newly developed isospin-dependent cluster recognition method has been reported to affect the production of light particles [22].

*liqf@hutczj.cn

The paper is arranged as follows. In the next section the new version of the ultrarelativistic quantum molecular dynamics (UrQMD) transport model with the Skyrme potential energy density functional is presented. In Sec. III, results of collective flows of light particles from $^{197}\text{Au} + ^{197}\text{Au}$ reactions at beam energies 150, 250, and 400 MeV/nucleon are shown. Finally, a summary and outlook are given in Sec. IV.

II. URQMD MODEL UPDATES

The UrQMD model [23–26] has been widely and successfully used to study pp , pA , and AA collisions within a large energy range from those used at Bevalac and SIS up to the energies available at the BNL Alternating Gradient Synchrotron (AGS), CERN Super Proton Synchrotron (SPS), BNL Relativistic Heavy Ion Collider (RHIC), and CERN Large Hadron Collider (LHC). At lower energies, the UrQMD model is based on principles analogous to the quantum molecular dynamics (QMD) model [27] in which each nucleon is represented by a Gaussian wave packet in phase space. The centroids \mathbf{r}_i and \mathbf{p}_i of a nucleon i in the coordinate and momentum spaces are propagated according to Hamilton's equations of motion:

$$\dot{\mathbf{r}}_i = \frac{\partial H}{\partial \mathbf{p}_i} \quad \text{and} \quad \dot{\mathbf{p}}_i = -\frac{\partial H}{\partial \mathbf{r}_i}. \quad (1)$$

The Hamiltonian H consists of the kinetic energy T and the effective two-body interaction potential energy U ,

$$H = T + U, \quad (2)$$

with

$$T = \sum_i (E_i - m_i) = \sum_i (\sqrt{m_i^2 + \mathbf{p}_i^2} - m_i), \quad (3)$$

and

$$U = U_\rho + U_{\text{md}} + U_{\text{Coul}}, \quad (4)$$

where U_{Coul} is the Coulomb energy, while the nuclear interaction potential energy terms U_ρ and U_{md} can be written as

$$U_{\rho,\text{md}} = \int u_{\rho,\text{md}} d\mathbf{r}. \quad (5)$$

In the current new version of the UrQMD model, the form of the momentum dependent term u_{md} is taken from the QMD model [27] while the Skyrme potential energy density functional u_ρ is introduced in the same manner as in the improved quantum molecular dynamics (ImQMD) model [28,29] in which

$$u_\rho = \frac{\alpha}{2} \frac{\rho^2}{\rho_0} + \frac{\beta}{\eta+1} \frac{\rho^{\eta+1}}{\rho_0^\eta} + \frac{g_{\text{sur}}}{2\rho_0} (\nabla\rho)^2 + \frac{g_{\text{sur,iso}}}{2\rho_0} [\nabla(\rho_n - \rho_p)]^2 + (A\rho^2 + B\rho^{\eta+1} + C\rho^{8/3})\delta^2 + g_{\rho\tau} \frac{\rho^{8/3}}{\rho_0^{5/3}}. \quad (6)$$

Here $\delta = (\rho_n - \rho_p)/(\rho_n + \rho_p)$ is the isospin asymmetry defined through the neutron (ρ_n) and proton (ρ_p) densities with $\rho = \rho_n + \rho_p$. The parameters α , β , η , g_{sur} , and $g_{\text{sur,iso}}$ are related to the Skyrme parameters via $\frac{\alpha}{2} = \frac{3}{8}t_0\rho_0$,

TABLE I. Saturation properties of the three Skyrme parametrizations used in this work.

	SkP [5,30]	SV-mas08 [5,31]	SkA [5,32]
ρ_0 (fm $^{-3}$)	0.163	0.160	0.155
E_0 (MeV)	-15.95	-15.90	-15.99
$S(\rho_0)$ (MeV)	30.00	30.00	32.91
L (MeV)	19.68	40.15	74.62
K_{asy} (MeV)	-266.60	-172.38	-78.46
m^*/m	1.00	0.80	0.61
K_0 (MeV)	201	233	263

$\frac{\beta}{\eta+1} = \frac{1}{16}t_3\rho_0^\eta$, $\frac{g_{\text{sur}}}{2} = \frac{1}{64}(9t_1 - 5t_2 - 4x_2t_2)\rho_0$, and $\frac{g_{\text{sur,iso}}}{2} = -\frac{1}{64}[3t_1(2x_1 + 1) + t_2(2x_2 + 1)]\rho_0$. The parameters A , B , and C in the volume symmetry energy term of Eq. (6) are given by $A = -\frac{t_0}{4}(x_0 + 1/2)$, $B = -\frac{t_2}{24}(x_3 + 1/2)$, and $C = -\frac{1}{24}(\frac{3\pi^2}{2})^{2/3}\Theta_{\text{sym}}$, where $\Theta_{\text{sym}} = 3t_1x_1 - t_2(4 + 5x_2)$. The last term reads $g_{\rho\tau} = \frac{3}{80}[3t_1 + (5 + 4x_2)t_2](\frac{3\pi^2}{2})^{2/3}\rho_0^{5/3}$. The coefficients t_0, t_1, t_2, t_3 and x_0, x_1, x_2, x_3 are the well-known parameters of the Skyrme force.

In this work, we choose three sets of the Skyrme force, SkP [5,30], SV-mas08 [5,31], and SkA [5,32], for incompressibility values K_0 varying within 230 ± 30 MeV. The main saturation properties of each set are listed in Table I which shows that the saturation density ρ_0 , the saturation energy E_0 , and the symmetry energy S_0 at ρ_0 are close to their commonly accepted values, 0.16 fm^{-3} , -16 MeV , and 32 MeV , respectively. The other three parameters, the slope L of the symmetry energy, the symmetry incompressibility K_{asy} , and the effective mass ratio m^*/m at ρ_0 , are also found within their known regions of uncertainty. It should be noticed that with the introduction of the ‘‘standard’’ Skyrme potential energy density functional, these parameters are not varied independently. But the effect of the isovector part of the EOS will not be much involved in this paper since its contribution to flows is much smaller than the isoscalar part of the EOS.

Concerning the NNCS, it is known that it will be modified by the nuclear medium, according to approaches such as the (self-consistent) relativistic Boltzmann-Uehling-Uhlenbeck (RBUU) and the (Dirac-)Brueckner-Hartree-Fock (DBHF), which are based on the theory of quantum hydrodynamics (QHD), see e.g., Refs. [33–37]. However, the details of this modification are still not clear. In this work, as done previously [25,38], the in-medium nucleon-nucleon elastic cross sections (NNECS) are treated to be factorized as the product of a medium correction factor F and the free cross sections. For the inelastic channels, we still use the experimental free-space cross sections which will not have a significant influence on results studied in this work. The total nucleon-nucleon binary scattering cross sections can thus be expressed as

$$\sigma_{\text{tot}}^* = \sigma_{\text{in}} + \sigma_{\text{el}}^* = \sigma_{\text{in}} + F(\rho, p)\sigma_{\text{el}}, \quad (7)$$

with

$$F(\rho, p) = \begin{cases} f_0 & p_{NN} > 1 \text{ GeV}/c, \\ \frac{F_\rho - f_0}{1 + (p_{NN}/p_0)^\kappa} + f_0 & p_{NN} \leq 1 \text{ GeV}/c, \end{cases} \quad (8)$$

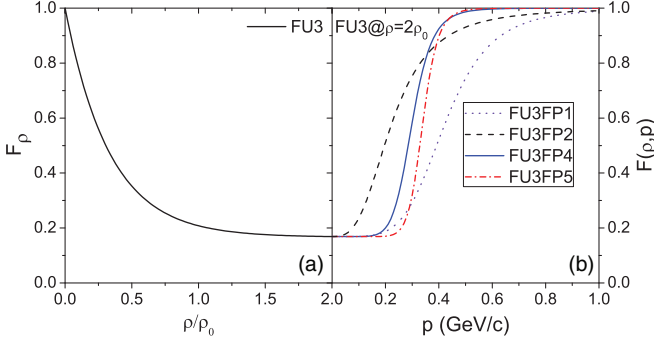


FIG. 1. (Color online) (a) The medium correction factor F_ρ obtained with the parametrization FU3 and (b) the momentum dependence with the four options FP1, FP2, FP4, and FP5 given in Table II for FU3 at $\rho = 2\rho_0$.

where p_{NN} denotes the relative momentum of two colliding nucleons. Here σ_{el} and σ_{in} are the nucleon-nucleon elastic and inelastic cross sections in free space, respectively, with the proton-neutron cross sections being considered as different from the proton-proton and neutron-neutron cross sections in accordance with experimental data. The factor F_ρ in Eq. (8) can be expressed as

$$F_\rho = \lambda + (1 - \lambda) \exp\left[-\frac{\rho}{\zeta\rho_0}\right], \quad (9)$$

which is also illustrated in Fig. 1(a). In this work, $\zeta = 1/3$ and $\lambda = 1/6$ are adopted, which corresponds to the parametrization FU3 in Ref. [25]. The three parameters f_0 , p_0 , and κ in Eq. (8) can be varied in order to obtain various momentum dependences of $F(\rho, p)$.

We select several parameter sets for this work which are shown in Table II. The corresponding $F(\rho, p)$ functions at $\rho = 2\rho_0$ are illustrated in Fig. 1(b). The parametrizations FP1, FP2, and FP3 were investigated and used in our previous works [25,39,40]. Specifically, the parameter set FU3FP1 was used to investigate HICs around the balance energy where the experimental data can be reproduced quite well with this set. Here, we further introduce the FP4 and FP5 sets which lie roughly between FP1 and FP2. This will permit more accurate tests of the momentum dependence of the in-medium NNCS by taking advantage of the large number of new FOPI data for directed and elliptic flows of light charged particles. FP4 and FP5 differ mainly within $p = 0.2 - 0.4$ GeV/c and the largest difference is within the narrow region $p = 0.25 - 0.35$ GeV/c.

TABLE II. The parameter sets FP1, FP2, FP3, FP4, and FP5 used for describing the momentum dependence of $F(u, p)$.

Set	f_0	p_0 (GeV/c)	κ
FP1	1	0.425	5
FP2	1	0.225	3
FP3	1	0.625	8
FP4	1	0.3	8
FP5	1	0.34	12

The treatment of the Pauli blocking effect is the same as that in Ref. [25].

The UrQMD transport program stops at 250 fm/c at which time a phase-space coalescence mode [41] is used to construct clusters. Usually, the minimum spanning tree (MST) algorithm is used. Recently, an isospin-dependent MST (iso-MST) method was introduced by Zhang *et al.* [22]. Accordingly, in this work we will apply the two methods of fragment recognition. The relative distance and momentum parameters R_0 and P_0 are set to $R_0^{nn} = R_0^{np} = R_0^{pp} = 3.2$ fm for MST and $R_0^{nn} = R_0^{np} = 4.5$ fm and $R_0^{pp} = 3.2$ fm for iso-MST, and $P_0 = 0.25$ GeV/c for both.

III. OBSERVABLES AND CALCULATIONS

A. What to calculate

Several hundred thousand events of $^{197}\text{Au} + ^{197}\text{Au}$ collisions for each of the beam energies $E_{lab} = 150, 250,$ and 400 MeV/nucleon are simulated randomly within the impact parameter region $0 - 7.5$ fm, in order for small enough statistical error bars for observables. As in Ref. [21], the centrality is characterized by the reduced impact parameter b_0 defined as $b_0 = b/b_{max}$, taking $b_{max} = 1.15(A_P^{1/3} + A_T^{1/3})$ fm = 13.4 fm for $^{197}\text{Au} + ^{197}\text{Au}$. At each beam energy, the calculations are divided into four groups according to b_0 : $b_0 < 0.15$, $0.15 < b_0 < 0.25$, $0.25 < b_0 < 0.45$, and $0.45 < b_0 < 0.55$ ($b_{max} \times 0.55 = 7.4$ fm). Five options of the UrQMD model differing in the treatment of the mean-field potential (EOS), the medium modified NNCS, and the cluster recognition method are adopted and listed in Table III. Clearly, the options UrQMD-I, UrQMD-IV, and UrQMD-V are for testing the influence of the mean-field potential, the options UrQMD-III and UrQMD-IV are for testing the in-medium NNCS, and UrQMD-II and UrQMD-IV are for testing the influence of the cluster recognition method.

As a general test of the model, we first calculated fragment spectra as a function of atomic number Z for central $^{197}\text{Au} + ^{197}\text{Au}$ collisions at beam energies $E_{lab} = 150, 250,$ and 400 MeV/nucleon. It is found that results obtained by the five UrQMD options listed in Table III are in agreement with experimental data and the differences among them are relatively small. As a sensitive observable to both the EOS and the in-medium NNECS [20,25], the nuclear stopping quantity $vartl$, defined by the FOPI Collaboration, of light charged clusters is investigated as well. One finds that results for flows and for nuclear stopping follow in the same order when

TABLE III. Five options of the UrQMD transport model differing in the treatments of the potential terms (EOS), of the medium-modified NNCS, and of the cluster recognition method.

Set	EOS	NNCS	Cluster recognition
UrQMD-I	SkP	FU3FP4	iso-MST
UrQMD-II	SV-mas08	FU3FP4	MST
UrQMD-III	SV-mas08	FU3FP5	iso-MST
UrQMD-IV	SV-mas08	FU3FP4	iso-MST
UrQMD-V	SkA	FU3FP4	iso-MST

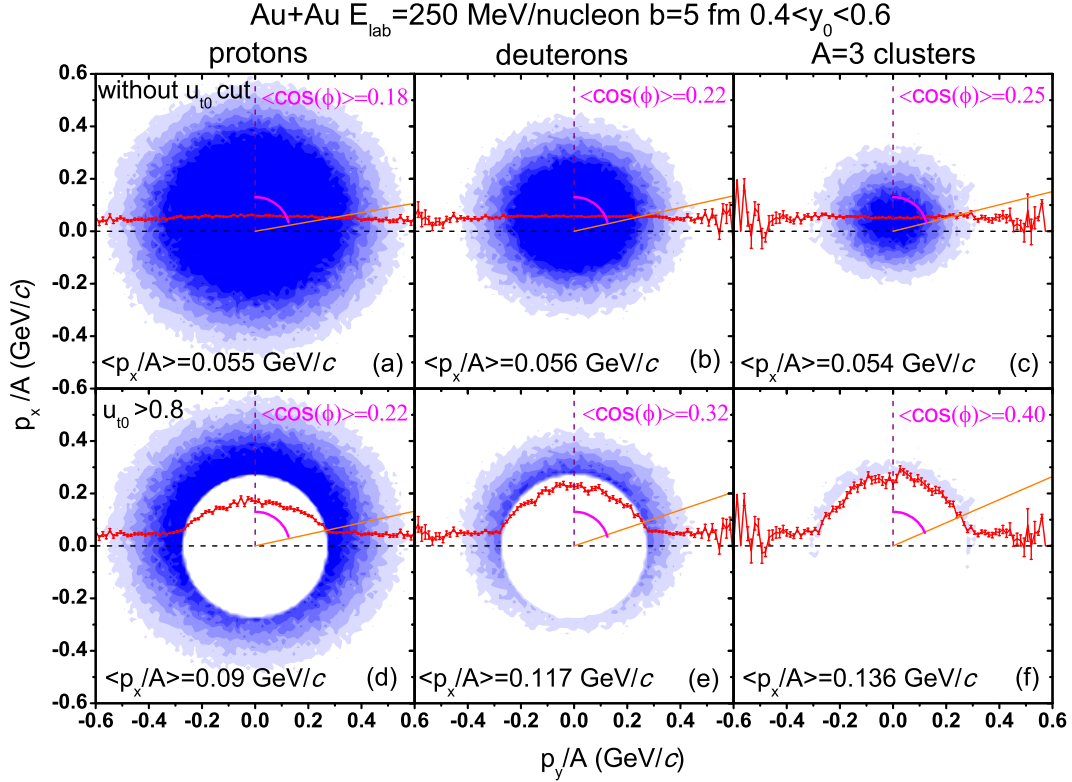


FIG. 2. (Color online) Contour plots of p_x/A vs p_y/A of free protons [left, (a) and (d)], deuterons [middle, (b) and (e)] and $A = 3$ clusters [right, (c) and (f)] calculated with UrQMD-IV and presented without a u_{t0} cut (upper row of panels) and with the cut $u_{t0} > 0.8$ (lower panels) for $^{197}\text{Au} + ^{197}\text{Au}$ reactions at 250 MeV/nucleon, $b = 5$ fm, and the bin of forward rapidities $0.4 < y_0 < 0.6$. The solid lines represent the averaged $\langle p_x \rangle / A$ value for each $\langle p_y \rangle / A$ bin, while the displayed numerical values in the lower part of each panel are the averages over the considered range of $\langle p_y \rangle / A$. Values of $\cos(\phi)$ are shown in the upper right corners of the panels.

different treatments of the mean field and the collision terms are chosen. However, details on nuclear stopping calculations will be published elsewhere later. Since the aim of this work is to explore whether more accurate constraints to the whole dynamic process of HICs can be obtained by comparing with the new flow data of the FOPI Collaboration, we will not present results on the fragment spectrum and on stopping power in this paper. It is known that one of the most important observables to constrain the stiffness of EOS of nuclear matter, especially at supra-normal densities, is the collective flow in HICs at intermediate energies. Using the same parametrization as in Ref. [21], we have

$$\frac{dN}{u_t du_t dy d\phi} = v_0 [1 + 2v_1 \cos(\phi) + 2v_2 \cos(2\phi)], \quad (10)$$

in which the directed and elliptic flow parameters v_1 and v_2 can be written as

$$v_1 \equiv \langle \cos(\phi) \rangle = \left\langle \frac{p_x}{p_t} \right\rangle, \quad v_2 \equiv \langle \cos(2\phi) \rangle = \left\langle \frac{p_x^2 - p_y^2}{p_t^2} \right\rangle. \quad (11)$$

Here ϕ is the azimuthal angle of the emitted particle with respect to the reaction plane, and $p_t = \sqrt{p_x^2 + p_y^2}$ is the transverse momentum of emitted particles. The angle brackets in Eq. (11) denote an average over all considered particles

from all events. The v_1 and v_2 have complex multi-dimensional dependences. For a certain reaction with fixed reaction system, beam energy, and impact parameter, they are functions of u_t and rapidity y . Here $u_t = \beta_t \gamma$ is the transverse component of the four-velocity $u = (\gamma, \beta \gamma)$. We use the scaled units $u_{t0} \equiv u_t / u_{1c.m.}$ and $y_0 \equiv y / y_{1c.m.}$ as done in Ref. [21], and the subscript 1c.m. denotes the incident projectile in the center-of-mass system.

We first investigate how the condition $u_{t0} > 0.8$, applied by FOPI to their data, influences the directed flow of different particles. In Fig. 2, the p_x/A vs p_y/A contour plots for emitted protons, deuterons, and $A = 3$ clusters (considering ^3H and ^3He results) are shown without the u_{t0} cut in the upper and with the cut $u_{t0} > 0.8$ in the lower panels. The interval of forward rapidities $0.4 < y_0 < 0.6$ is selected, so that more particles have positive p_x . The solid lines represent the averaged $\langle p_x \rangle / A$ values for each p_y/A bin and the numerical values in the lower part of the panels are the averages over all considered p_y/A bins. In the upper right corner of each panel, the averaged value of $\cos(\phi)$ ($=v_1$) for separate particles is also shown for comparison. It is apparent from Figs. 2(a)–2(c) that the $\langle p_x \rangle / A$ values of protons, deuterons, and $A = 3$ clusters are the same when the u_{t0} cut is not taken into account. When the cut $u_{t0} > 0.8$ is applied, however, shown in Figs. 2(d)–2(f), the $\langle p_x \rangle / A$ value increases with increasing particle mass. If, however, the value of v_1 is examined, heavier clusters have

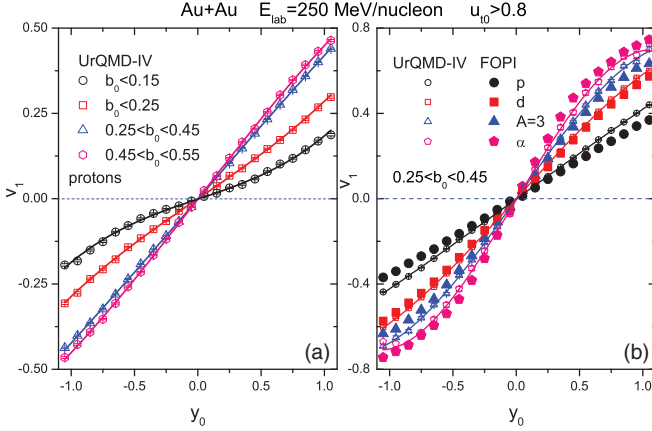


FIG. 3. (Color online) Rapidity distribution of (a) the flow parameter v_1 of protons under various centralities and (b) flow parameter v_1 for protons, deuterons, $A = 3$ clusters, and α particles from $^{197}\text{Au} + ^{197}\text{Au}$ collisions at 250 MeV/nucleon with $0.25 < b_0 < 0.45$, as calculated with the UrQMD-IV option (open symbols). The cut $u_{t0} > 0.8$ is chosen. The lines are fits to the calculation results (see text), while the corresponding experimental data from Ref. [21] are given by the solid symbols.

larger transverse flow, even though there is not any u_{t0} cut. With the consideration of the u_{t0} cut, the effect of the particle species on flow becomes even more remarkable. This shows that the expected collective proportionality to the particle mass is observed when all particles are included and suggests that the phenomenon of an additional increase of the flow effect with the particle mass is strongly correlated with whether a transverse momentum cut is applied or not.

Now, let us look at the collective flow as a function of rapidity when a u_{t0} cut is applied. Figure 3 shows the directed flow v_1 of protons under different centralities (open symbols) in plot (a), and v_1 of protons, deuterons, $A = 3$, and α particles (open symbols) with the centrality $0.25 < b_0 < 0.45$ in (b) as a function of y_0 . The UrQMD-IV is adopted for calculations, the reaction conditions in Fig. 3(b) are chosen to be the same as the FOPI experimental data (solid symbols) of Ref. [21]. The solid curves in the figure are fits to calculation results assuming $v_1(y_0) = v_{11}y_0 + v_{13}y_0^3 + c$ in the range of $-1.1 < y_0 < 1.1$. The fit also provides the slope value v_{11} of v_1 at $y_0 = 0$ which will be discussed later. In Fig. 3(b), it is found that our calculated results for all particles considered are in agreement with the experimental data in the whole rapidity region.

The elliptic flow v_2 of light particles is also calculated and compared with FOPI data from Ref. [21]. In Fig. 4, the results of calculations with UrQMD-IV and the FOPI data from $^{197}\text{Au} + ^{197}\text{Au}$ collisions at 400 MeV/nucleon are represented by the open and solid symbols, respectively. In Fig. 4(a), the elliptic flow parameter v_2 of protons as a function of y_0 is shown for three centralities, while the v_2 for different particles, i.e., protons, deuterons and α particles, is given in Fig. 4(b) (for semi-central collisions and with the less restrictive u_{t0} cut applied by FOPI at the higher energy). The figure shows that the FOPI v_2 flow data, within a large centrality region and for several particles, can also be quite well described with

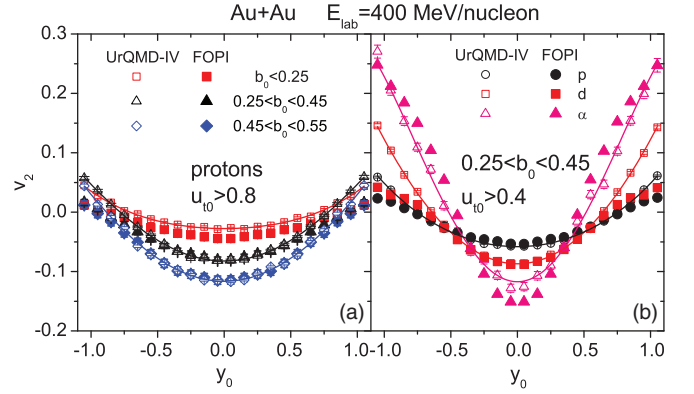


FIG. 4. (Color online) Rapidity distribution of the flow parameter v_2 of protons for various centralities (a) and the v_2 of protons, deuterons, and α particles for the impact-parameter bin $0.25 < b_0 < 0.45$ for $^{197}\text{Au} + ^{197}\text{Au}$ collisions at 400 MeV/nucleon. Calculations with UrQMD-IV are shown with open symbols while the FOPI data, taken from Ref. [21], are shown by solid symbols. The lines are fits to the calculated results (see text).

the updated UrQMD transport model. Further, with the fit $v_2(y_0) = v_{20} + v_{22}y_0^2 + v_{24}y_0^4$ to the calculation, the elliptic flow at mid-rapidity, v_{20} , can be obtained.

B. Effects of EOS, NNCS, and cluster recognition on flows of light particles

To show why the sets FP4 and FP5 have been introduced in addition to FP1 and FP2 used previously for testing the momentum dependence of the in-medium NNCS, we display in Fig. 5(a) the v_{11} and in Fig. 5(b) the v_{20} values for light particles calculated with the four sets FP1, FP2, FP4, and FP5. Other inputs are the same as those in the UrQMD-IV set. First, one sees clearly that calculation results with FP4 and FP5 are well separated. It means that the directed and elliptic flows of light particles are very sensitive to the exact momentum dependence of in-medium NNCS within a narrow

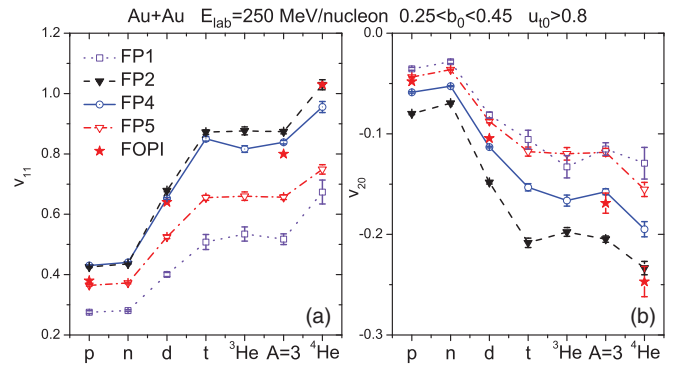


FIG. 5. (Color online) (a) v_{11} and (b) v_{20} values for light particles up to mass number $A = 4$ calculated with FP1, FP2, FP4, and FP5 (lines with symbols) while other inputs are the same as those in the UrQMD-IV set. The reaction $^{197}\text{Au} + ^{197}\text{Au}$ at the beam energy 250 MeV/nucleon with $0.25 < b_0 < 0.45$ is considered as an example. The FOPI experimental data (stars) are taken from Ref. [21].

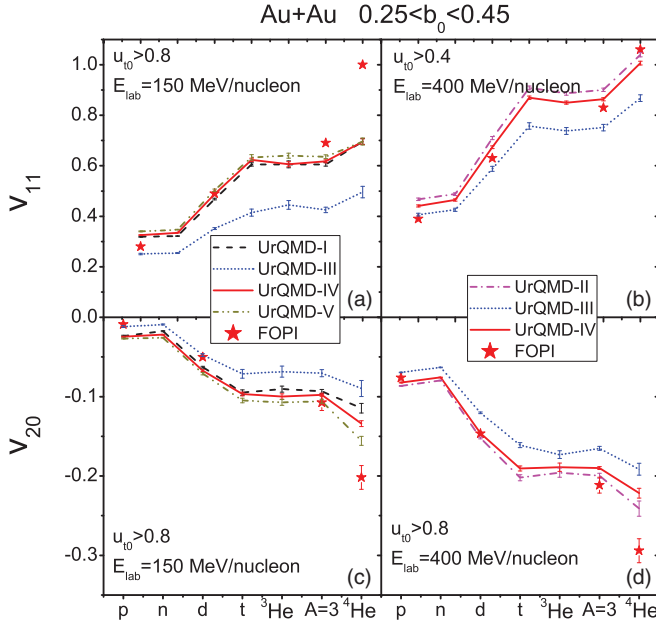


FIG. 6. (Color online) v_{11} [(a) and (b)] and v_{20} [(c) and (d)] for light particles from semi-central ($0.25 < b_0 < 0.45$) $^{197}\text{Au} + ^{197}\text{Au}$ collisions at $E_{\text{lab}} = 150$ (left) and 400 MeV/nucleon (right). The calculations performed with five UrQMD parameter sets are distinguished by different lines as indicated. The FOPI experimental data from Ref. [21] are shown by stars.

region of $p = 0.2\text{--}0.4$ GeV/ c , which is due to a larger number of collisions happening in such a relative momentum region. Second, the v_{11} of light particles calculated with FP2 and FP4 and the v_{20} calculated with FP1 and FP5 are very close to each other, respectively. Remembering that there is a large difference between FP2 and FP4 at the low momentum part and between FP1 and FP5 at high momenta (see Fig. 1), we may conclude that the directed flow of light particles is not sensitive to the low momentum part while the elliptic flow is not sensitive to the high momentum part of the momentum dependent NNECS. However, with the further increase of beam energy, the sensitivity of the collective flow to the parametrization FP4 and FP5 will be reduced since they overlap at higher relative momentum (which is also shown in Fig. 6). The figure finally also shows that the calculations with FP4 can best reproduce the experimental data.

Besides the medium modification on NNECS, also the influence of the mean field and of the cluster recognition method on flows is further investigated. In Fig. 6, the v_{11} and v_{20} values obtained from calculations with different UrQMD sets for light particles from semi-central $^{197}\text{Au} + ^{197}\text{Au}$ collisions at two beam energies, 150 (left) and 400 MeV/nucleon (right), are compared with the FOPI data. More specifically, the mean-field effect is examined in Figs. 6(a) and 6(c) where calculations with UrQMD-I, UrQMD-III, UrQMD-IV, and UrQMD-V sets are shown, while the cluster recognition effect is tested in Figs. 6(b) and 6(d) with calculations using the UrQMD-II, UrQMD-III, and UrQMD-IV sets. One immediately sees that for both v_{11} and v_{20} , calculations with UrQMD-I, UrQMD-II, UrQMD-IV,

and UrQMD-V are grouped together, while absolute values obtained with UrQMD-III are apparently smaller, especially for composite particles. The main reason is that with FP5, the reduction of the in-medium cross section is stronger in the UrQMD-III case. Flows of composite particles at intermediate energies are, apparently, very useful to test the behavior of the momentum dependence of in-medium NNECS, especially in the momentum region $p = 0.2\text{--}0.4$ GeV/ c . Second, although the absolute values of v_{11} and v_{20} are still seen to increase gradually with the increasing incompressibility K_0 of the EOS, by examining calculations going from UrQMD-I, UrQMD-IV, to UrQMD-V sets, the differences between them are too small to extract a more accurate K_0 value than 230 ± 30 MeV from the present calculations and experimental data. By employing a much stiffer EOS such as SIII (with $K_0 = 355$ MeV), we have checked that the sensitivity of the flows to the EOS is comparable with previous studies shown, e.g., Ref. [2]. The insensitivity of the flows to the EOS shown here is only because the selected range of K_0 values is rather narrow based on the latest progress on it. It is further noticed that although the effective mass values of the three Skyrme forces are largely different, the flow is not influenced significantly. This is because the momentum dependent terms in the Skyrme potential energy density functional are obtained by the Thomas-Fermi approximation to the kinetic energy density and cannot fully represent the momentum dependence of the whole non-equilibrium dynamic process.

We note that to obtain an improved flow data set of light fragments for $^{197}\text{Au} + ^{197}\text{Au}$ collisions and to extend the study of the density dependent symmetry energy to other systems, a new experiment (S394) was recently carried out at the GSI laboratory by the ASY-EOS Collaboration [42]. It is certainly hopeful for us to further reduce the uncertainties in both K_0 and K_{asy} with the help of the new experiment.

Finally, from Figs. 6(b) and 6(d) one finds that no matter which flow parameter is chosen, the difference between results calculated with UrQMD-II and with UrQMD-IV is also very small. And the flow parameter difference in some isospin partners such as proton+neutron and $^3\text{He} + ^3\text{H}$ is not obvious as well. It indicates that the different cluster recognition methods MST and iso-MST have only a weak effect on the flow parameters. However, the effect should depend on the transverse momentum and rapidity cuts [as will be seen in Fig. 7(c), the difference in v_1 between MST and iso-MST becomes larger as u_{t0} decreases]. Since both MST and iso-MST are different treatments related to isospin in the coalescence model at freeze-out, it has been found in Ref. [22] that yields of neutron-rich lighter fragments as well as isospin-dependent observables such as yield ratios between isospin partners are influenced. Similarly, the flow difference or ratio between isospin partners in some transverse momentum and/or rapidity windows might be influenced by the consideration of isospin in MST, which deserves further investigation. Generally speaking, we can conclude that the new FOPI flow data can be reproduced by the UrQMD model calculations when the FU3FP4 medium modification of NNECS is adopted, with the only exception of α particle flow, which is underestimated. Reasons for the underestimation will be discussed in the next section.

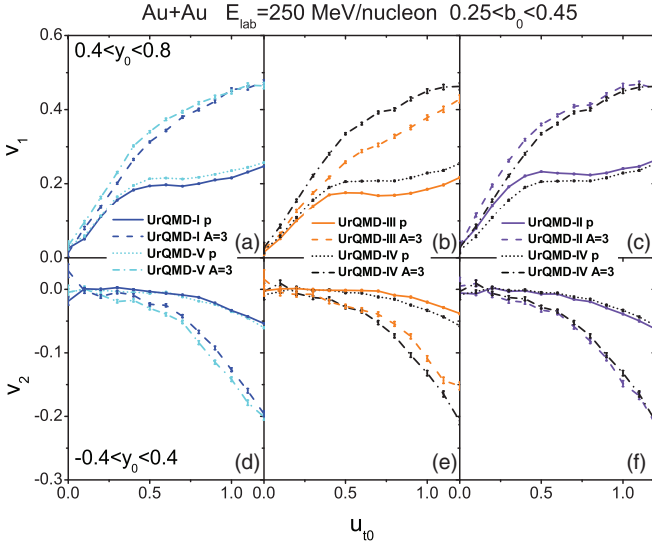


FIG. 7. (Color online) Parameters v_1 of directed flow (upper panels) and v_2 of elliptic flow (lower panels) for protons and $A = 3$ clusters as a function of u_{t0} . Calculations are obtained with UrQMD-I and UrQMD-V in (a) and (d), UrQMD-III and UrQMD-IV in (b) and (e), and UrQMD-II and UrQMD-IV in (c) and (f). The reaction $^{197}\text{Au} + ^{197}\text{Au}$ at the beam energy 250 MeV/nucleon with $0.25 < b_0 < 0.45$ is considered as an example. The rapidity cuts $0.4 < y_0 < 0.8$ and $|y_0| < 0.4$ are chosen for v_1 and v_2 , respectively.

To see more clearly effects of the mean-field potential, the in-medium NNCS, and the cluster recognition method on flows, the calculated parameters v_1 of directed and v_2 of elliptic flow are shown as a function of u_{t0} in Fig. 7. For this purpose, we compare results of protons and $A = 3$ clusters obtained with UrQMD-I and UrQMD-V in Figs. 7(a) and 7(d), with UrQMD-III and UrQMD-IV in Figs. 7(b) and 7(e), and with UrQMD-II and UrQMD-IV in Figs. 7(c) and 7(f). As an example, $^{197}\text{Au} + ^{197}\text{Au}$ collisions at the beam energy 250 MeV/nucleon with $0.25 < b_0 < 0.45$ are chosen. One sees a significant effect on both flow parameters only in the case of the comparison of calculations with UrQMD-III to UrQMD-IV shown in Figs. 7(b) and 7(e), especially for $A = 3$ clusters. This situation is quite similar to that shown in Fig. 6. Further, it can be seen from Fig. 7 that at about $u_{t0} > 0.5$ the effect of medium modified NNCS on flows of $A = 3$ clusters is enlarged [from Figs. 7(b) and 7(e)] while the other two effects are reduced so that one may be able to more cleanly determine the medium modifications of NNCS in this momentum region.

C. Comparison of calculated u_{t0} dependent flows to experimental data

We finally show in Fig. 8 the u_{t0} dependence of calculated directed (left panels) and elliptic flows (right panels) of light charged particles at beam energies 150, 250, and 400 MeV/nucleon (lines). The reaction system and chosen rapidity cuts are the same as for the experimental data taken from Ref. [21] and shown by the full symbols. It is first observed that calculations with the UrQMD-IV set reproduce the v_1 and v_2 data reasonably well with some exceptions.

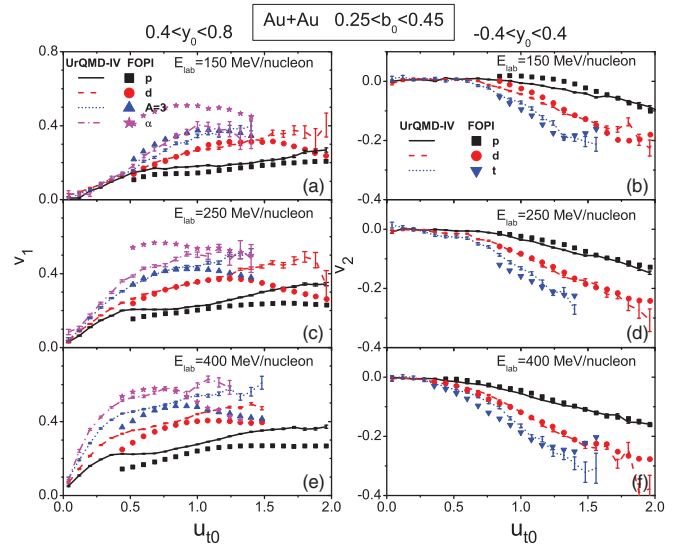


FIG. 8. (Color online) The u_{t0} dependence of parameters v_1 of directed (left) and v_2 of elliptic flows (right) of light charged particles from semi-central ($0.25 < b_0 < 0.45$) $^{197}\text{Au} + ^{197}\text{Au}$ collisions at beam energies 150, 250, and 400 MeV/nucleon. The rapidity cuts $0.4 < y_0 < 0.8$ and $|y_0| < 0.4$ are chosen for v_1 and v_2 , respectively. Calculated results with UrQMD-IV are represented by different lines as indicated, the FOPI experimental data from Ref. [21] are shown by solid symbols.

Although the experimental data of directed flow of α particles cannot be well described by the model, the relatively large flow effect is clearly exhibited in Figs. 8(a), 8(c), and 8(e). Second, calculation results for absolute v_1 and v_2 values of protons are slightly larger than the FOPI data, which is similar to the simulation results shown in Ref. [21] where the isospin quantum molecular dynamics (IQMD) model was used. Third, when u_{t0} is larger than about 1.0, the deviation of the calculated v_1 from the data starts to increase in some of the particle cases. Although, on the other hand, the yields of these particles are quite small in these u_{t0} and y_0 regions, and the contribution to the final v_{t1} value is thus very limited. One has indeed seen the successful description of the u_{t0} -integrated data by the UrQMD-IV set shown in Fig. 6.

To our knowledge, the discrepancies shown above can be (partly) understood for three reasons: (1) it is argued that largely due to simplifications in the initial wave function of particles (nucleons and possible clusters) and quantum effects in two-body collisions, the yield of free nucleons (intermediate mass fragments, especially α particles), is largely overestimated (underestimated) by QMD. And because of the strong decay of excited fragments, flows of lighter particles will definitely inherit partly those of their heavier parent fragments. Therefore, some of the free nucleons might thus actually belong to fragments. Since the flow effect is larger for fragments than for emitted nucleons, the calculated flows of free protons are consequently overestimated. As for the α particle, however, the calculated flows are mostly underestimated, especially at small u_{t0} for HICs at lower beam energies [as can be seen in Fig. 8(a)], which might be due to its deficiency of production from heavier excited fragments

and its instability after production in model calculations. To improve the α particle estimates, the antisymmetrized molecular dynamics model (AMD) has been developed and is being kept updated [43,44]. (2) The importance of the optical potential to observables such as particle production and flow measured in HICs at intermediate energies has been widely investigated but its form is still far from settled [45–47]. And (3) the treatment of the fragment production could be more comprehensive than the current constraints in the phase space besides the consideration of the isospin. For example, to describe the early formation of fragments, the simulated annealing clusterization algorithm (SACA) [48], which is based on the energy minimization criteria, was proposed and shown to be promising.

Finally, as for flows of deuterons and $A = 3$ clusters, it is seen that the comparison of UrQMD-IV calculations with the experimental data is fairly good in the range $0.5 < u_{t0} < 1.0$. In view of the result shown in Fig. 7, it is highly advantageous to investigate the detailed behavior of the medium corrected NNCS in this momentum region. In order for a more reliable comparison to data, some recently concerned issues in the community, i.e., the internal magnetic fields [49] and non-central forces as, e.g., the tensor force and spin-orbit coupling [50,51] which might influence the freeze-out mode of HICs especially for non-central collisions at large momenta and rapidities, will be further studied within the same transport theory.

IV. SUMMARY AND OUTLOOK

In summary, we have studied the directed and elliptic flows of light particles in $^{197}\text{Au} + ^{197}\text{Au}$ collisions at beam energies 150, 250, and 400 MeV/nucleon by using the updated UrQMD model in which the Skyrme potential energy density functional

is introduced. After the detailed study of the influence of equation of state (EOS), medium-modified nucleon-nucleon elastic cross section (NNECS) and cluster recognition criteria on flows, the three questions asked in the Introduction can be answered: (1) it is difficult to get a more exact value of the incompressibility from the present flow data than $K_0 = 230 \pm 30$ MeV, (2) the different choices of medium-modified NNECS exhibit a significant influence on the light particle flows and, particularly, on the flows of light composite particles, and (3) the influence of the cluster recognition method on cluster flows is weak. The version of UrQMD-IV, comprising the SV-mas08 force with a corresponding incompressibility $K_0 = 234$ MeV, the FU3FP4 medium-modified NNECS, and the iso-MST cluster recognition method, describes the directed and elliptic flows of light particles as functions of both rapidity and transverse momentum rather well.

Theoretically, the spin-orbit coupling term in the Skyrme interactions will be further put into the UrQMD transport model after incorporating the spin degree of freedom and its contribution to flows, especially at large rapidities and/or transverse momenta, for intermediate energy HICs can then be identified. Together with the forthcoming new flow data of light particles measured by the ASY-EOS Collaboration at GSI, we hope to further reduce the uncertainties in both K_0 and K_{asy} of the isospin-dependent EOS within the present framework of UrQMD in the near future.

ACKNOWLEDGMENTS

We acknowledge support by the computing server C3S2 in Huzhou Teachers College. The work is supported in part by the National Natural Science Foundation of China (Nos. 11375062, 11175074, 11075215, 11275052), the project sponsored by SRF for ROCS, SEM, and the National Key Basic Research Program of China (No.2013CB834400).

-
- [1] B. A. Li, L. W. Chen, and C. M. Ko, *Phys. Rep.* **464**, 113 (2008).
 - [2] P. Danielewicz, R. Lacey, and W. G. Lynch, *Science* **298**, 1592 (2002).
 - [3] W. Reisdorf and H. G. Ritter, *Annu. Rev. Nucl. Part. Sci.* **47**, 663 (1997).
 - [4] C. T. Sturm *et al.* (KAOS Collaboration), *Phys. Rev. Lett.* **86**, 39 (2001); C. Fuchs, A. Faessler, E. Zabrodin, and Y.-M. Zheng, *ibid.* **86**, 1974 (2001); C. Hartnack, H. Oeschler, and J. Aichelin, *ibid.* **96**, 012302 (2006).
 - [5] M. Dutra, O. Lourenco, J. S. Sa Martins, A. Delfino, J. R. Stone, and P. D. Stevenson, *Phys. Rev. C* **85**, 035201 (2012).
 - [6] K. G. R. Doss, H. A. Gustafsson, H. Gutbrod, J. W. Harris, B. V. Jacak, K. H. Kampert, B. Kolb, A. M. Poskanzer *et al.*, *Phys. Rev. Lett.* **59**, 2720 (1987).
 - [7] H. H. Gutbrod, A. M. Poskanzer, and H. G. Ritter, *Rep. Prog. Phys.* **52**, 1267 (1989).
 - [8] H. H. Gutbrod, K. H. Kampert, B. Kolb, A. M. Poskanzer, H. G. Ritter, R. Schicker, and H. R. Schmidt, *Phys. Rev. C* **42**, 640 (1990).
 - [9] G. D. Westfall, W. Bauer, D. Craig, M. Cronqvist, E. Gaultieri, S. Hannuschke, D. Klakow, T. Li *et al.*, *Phys. Rev. Lett.* **71**, 1986 (1993).
 - [10] M. D. Partlan *et al.* (EOS Collaboration), *Phys. Rev. Lett.* **75**, 2100 (1995).
 - [11] M. J. Huang, R. C. Lemmon, F. Daffin, W. G. Lynch, C. Schwarz, M. B. Tsang, C. Williams, P. Danielewicz *et al.*, *Phys. Rev. Lett.* **77**, 3739 (1996).
 - [12] F. Rami *et al.* (FOPI Collaboration), *Nucl. Phys. A* **646**, 367 (1999).
 - [13] J. Barrette *et al.* (E877 Collaboration), *Phys. Rev. C* **59**, 884 (1999).
 - [14] G. Peilert, H. Stöcker, W. Greiner, A. Rosenhauer, A. Bohnet, and J. Aichelin, *Phys. Rev. C* **39**, 1402 (1989).
 - [15] V. Koch, B. Blättel, W. Cassing, U. Mosel, and K. Weber, *Phys. Lett. B* **241**, 174 (1990).
 - [16] J. Zhang and C. Gale, *Phys. Rev. C* **51**, 1425 (1995).
 - [17] P. Danielewicz, *Phys. Rev. C* **51**, 716 (1995).
 - [18] J. Nemeth, G. Papp, and H. Feldmeier, *Nucl. Phys. A* **647**, 107 (1999).

- [19] A. Insolia, U. Lombardo, and N. Sandulescu, *Phys. Rev. C* **61**, 067902 (2000).
- [20] W. Reisdorf *et al.* (FOPI Collaboration), *Nucl. Phys. A* **848**, 366 (2010).
- [21] W. Reisdorf *et al.* (FOPI Collaboration), *Nucl. Phys. A* **876**, 1 (2012).
- [22] Y. Zhang, Z. Li, C. Zhou, and M. B. Tsang, *Phys. Rev. C* **85**, 051602 (2012).
- [23] S. A. Bass *et al.* (UrQMD Collaboration), *Prog. Part. Nucl. Phys.* **41**, 255 (1998).
- [24] M. Bleicher, E. Zabrodin, C. Spieles, S. A. Bass, C. Ernst, S. Soff, L. Bravina, M. Belkacem *et al.*, *J. Phys. G* **25**, 1859 (1999).
- [25] Q. Li, C. Shen, C. Guo, Y. Wang, Z. Li, J. Lukasik, and W. Trautmann, *Phys. Rev. C* **83**, 044617 (2011).
- [26] Q. Li, G. Graf, and M. Bleicher, *Phys. Rev. C* **85**, 034908 (2012).
- [27] J. Aichelin, *Phys. Rep.* **202**, 233 (1991).
- [28] Y. Zhang and Z. Li, *Phys. Rev. C* **74**, 014602 (2006).
- [29] Y. Zhang, Z. Li, and P. Danielewicz, *Phys. Rev. C* **75**, 034615 (2007).
- [30] J. Dobaczewski, H. Flocard, and J. Treiner, *Nucl. Phys. A* **422**, 103 (1984).
- [31] P. Klupfel, P. G. Reinhard, T. J. Burvenich, and J. A. Maruhn, *Phys. Rev. C* **79**, 034310 (2009).
- [32] H. S. Köhler, *Nucl. Phys. A* **258**, 301 (1976).
- [33] K.-C. Chou, Z.-B. Su, B.-L. Hao, and L. Yu, *Phys. Rep.* **118**, 1 (1985).
- [34] G. Mao, Z. Li, Y. Zhuo, Y. Han, and Z. Yu, *Phys. Rev. C* **49**, 3137 (1994).
- [35] Q. Li, Z. Li, and G. Mao, *Phys. Rev. C* **62**, 014606 (2000); Q. Li, Z. Li, and E. Zhao, *ibid.* **69**, 017601 (2004).
- [36] G. Q. Li and R. Machleidt, *Phys. Rev. C* **48**, 1702 (1993); **49**, 566 (1994).
- [37] F. Sammarruca and P. Krastev, *Phys. Rev. C* **73**, 014001 (2006).
- [38] Q. Li, Z. Li, S. Soff, M. Bleicher, and H. Stöcker, *J. Phys. G* **32**, 407 (2006).
- [39] C. Guo, Y. Wang, Q. Li, W. Trautmann, L. Liu, and L. Wu, *Sci. China Phys. Mech. Astron.* **55**, 252 (2012).
- [40] Y. Wang, C. Guo, Q. Li, and H. Zhang, *Sci. China Phys. Mech. Astron.* **55**, 2407 (2012).
- [41] H. Kruse, B. V. Jacak, J. J. Molitoris, G. D. Westfall, and H. Stöcker, *Phys. Rev. C* **31**, 1770 (1985).
- [42] P. Russotto *et al.* (ASY-EOS Collaboration), *J. Phys. Conf. Ser.* **420**, 012092 (2013).
- [43] Ono Akira and H. Horiuchi, *Prog. Part. Nucl. Phys.* **53**, 501 (2004).
- [44] Y. Kanada-En'yo, M. Kimura, and A. Ono, *Prog. Theor. Exp. Phys.* (2012) 01A202.
- [45] J. Aichelin, A. Rosenhauer, G. Peilert, H. Stoecker, and W. Greiner, *Phys. Rev. Lett.* **58**, 1926 (1987).
- [46] C. Hartnack and J. Aichelin, *Phys. Rev. C* **49**, 2801 (1994).
- [47] L. W. Chen, C. M. Ko, and B. A. Li, *Phys. Rev. Lett.* **94**, 032701 (2005).
- [48] R. K. Puri, C. Hartnack, and J. Aichelin, *Phys. Rev. C* **54**, R28 (1996).
- [49] L. Ou and B. A. Li, *Phys. Rev. C* **84**, 064605 (2011).
- [50] C. Xu and B. A. Li, *Phys. Rev. C* **81**, 064612 (2010).
- [51] J. Xu and B. A. Li, *Phys. Lett. B* **724**, 346 (2013).